

# HS 2231+2441: an HW Vir system composed of a low-mass white dwarf and a brown dwarf<sup>\*</sup>

L. A. Almeida,<sup>1,2★</sup> A. Daminieli,<sup>1</sup> C. V. Rodrigues,<sup>3★</sup> M. G. Pereira<sup>4</sup> and F. Jablonski<sup>3</sup>

<sup>1</sup>Instituto de Astronomia, Geofísica e Ciências Atmosféricas Rua do Matão 1226, Cidade Universitária São Paulo-SP, 05508-090, Brazil

<sup>2</sup>Universidade Federal do Rio Grande do Norte, UFRN, Departamento de Física, CP 1641, Natal, RN, 59072-970, Brazil

<sup>3</sup>Instituto Nacional de Pesquisas Espaciais/MCTIC Avenida dos Astronautas 1758, São José dos Campos, SP, 12227-010, Brazil

<sup>4</sup>Departamento de Física, Universidade Estadual de Feira de Santana Av. Transnordestina, S/N, Feira de Santana, BA, 44036-900, Brazil

Accepted 2017 August 16. Received 2017 August 15; in original form 2017 May 28

## ABSTRACT

HW Vir systems are rare evolved eclipsing binaries composed of a hot compact star and a low-mass main sequence star in a close orbit. These systems provide a direct way to measure the fundamental properties, e.g. masses and radii, of their components, hence they are crucial in studying the formation of subdwarf B stars and low-mass white dwarfs, the common-envelope phase and the pre-phase of cataclysmic variables. Here, we present a detailed study of HS 2231+2441, an HW Vir type system, by analysing  $BVR_CI_C$  photometry and phase-resolved optical spectroscopy. The spectra of this system, which are dominated by the primary component features, were fitted using non-local thermodynamic equilibrium models providing an effective temperature  $T_{\text{eff}} = 28\,500 \pm 500$  K, surface gravity  $\log g = 5.40 \pm 0.05$  cm s<sup>-2</sup> and helium abundance  $\log(n(\text{He})/n(\text{H})) = -2.52 \pm 0.07$ . The geometrical orbit and physical parameters were derived by simultaneously modelling the photometric and spectroscopic data using the Wilson–Devinney code. We derive two possible solutions for HS 2231+2441 that provide the component masses:  $M_1 = 0.19 M_{\odot}$  and  $M_2 = 0.036 M_{\odot}$  or  $M_1 = 0.288 M_{\odot}$  and  $M_2 = 0.046 M_{\odot}$ . Considering the possible evolutionary channels for forming a compact hot star, the primary of HS 2231+2441 probably evolved through the red-giant branch scenario and does not have a helium-burning core, which is consistent with a low-mass white dwarf. Both solutions are consistent with a brown dwarf as the secondary.

**Key words:** binaries: eclipsing – brown dwarfs – stars: fundamental parameters – stars: individual: HS 2231+2441 – white dwarfs.

## 1 INTRODUCTION

HW Vir systems are evolved eclipsing binaries with a short orbital period and composed of a hot compact star and a low-mass main sequence star. In the most plausible scenario for forming these systems, the progenitor of the hot compact star evolves faster than the secondary (a low-mass main sequence star), which starts an unstable mass transfer phase and subsequently there is a common envelope. During the common-envelope stage, the secondary spirals in towards the primary and the released gravitational potential energy is absorbed by the envelope, which is subsequently ejected (Taam & Sandquist 2000; Han et al. 2002, 2003). The final geometrical configuration between the components depends on the initial mass

ratio and separation. These objects are rare, and only a few dozen systems are known so far (see e.g. Almeida et al. 2012; Østensen et al. 2013; Schafferoth et al. 2014; Heber 2016). As they provide a direct way to measure the geometrical and physical properties of the components, detailed studies of such systems are crucial for testing the theories on the formation and evolution of these kind of systems. For a recent review of HW Vir systems, see Heber (2016).

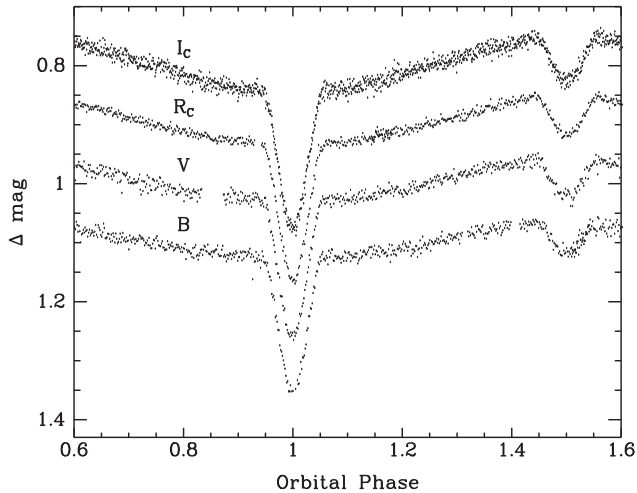
The primary star in HW Vir may be classified as one of three types: a hot subdwarf B (sdB) star, a low-mass white dwarf (LMWD) or an extremely low-mass (ELM) white dwarf, which depends essentially on how much mass was stripped from the primary star during the common-envelope phase and how massive is the remaining core. While sdB are core helium-burning stars with a canonical mass of approximately  $0.47 M_{\odot}$ , LMWDs and ELM white dwarfs do not have enough mass to ignite the helium (He) in their cores. LMWDs and ELM white dwarfs have a mass around  $0.3 M_{\odot}$  and  $0.2 M_{\odot}$  (Brown et al. 2010; Heber 2016), respectively. The spectra of sdBs, LMWDs and ELM white dwarfs are very similar: all of them populate the extreme horizontal branch (EHB) and its neighborhood in the Hertzsprung–Russell diagram. Therefore,

<sup>\*</sup> Based on observations carried out at the Observatório do Pico dos Dias (OPD/LNA) in Brazil and with the William Herschel Telescope at the Observatorio del Roque de los Muchachos.

<sup>\*</sup> E-mail: leonardodealmeida.andrade@gmail.com (LAA); claudia.rodrigues@inpe.br (CVR)

**Table 1.** Log of the photometric observations of HS 2231+2441.

Date	$N$	$t_{\text{exp}}$ (s)	Telescope	Filter
2010 Aug 19	300	30	0.6-m	$R_C$
2010 Aug 20	295	30	0.6-m	$V$
2011 Jul 07	650	10	1.6-m	$R_C$
2011 Jul 08	840	10	1.6-m	$I_C$
2011 Aug 15	900	5	1.6-m	$B$
2012 Aug 08	600	10	1.6-m	$V$
2012 Aug 09	630	10	1.6-m	$B$
2013 Jul 29	644	5	1.6-m	$I_C$
2013 Aug 01	1230	4	1.6-m	$I_C$

**Figure 1.** Normalised light curves of HS 2231+2441 in the  $B$ ,  $V$ ,  $R_C$  and  $I_C$  bands folded on the 0.1105879 d orbital period. The light curves have arbitrary displacements in  $\Delta$  mag for better visualization.

it is necessary to estimate the mass of the primary to identify correctly its evolutionary status.

HS 2231+2441 (2MASS J22342148+2456573) is an HW Vir system with an orbital period of  $\sim 0.1$  d. This system was described in two conference papers by Østensen et al. (2007, 2008). In the first study, the authors showed two possible solutions for this system using one photometric band and 27 epochs of spectroscopic data. They concluded that the most plausible solution provides a secondary mass of  $0.075 M_{\odot}$ , when considering a canonical mass  $0.470 M_{\odot}$  for the primary star. In the second one, Østensen et al. (2008) presented a new solution by analysing the same data set and obtained masses less than  $0.3 M_{\odot}$  and  $0.10 M_{\odot}$  for the primary and secondary, respectively.

In this study, we improve the solution for HS 2231+2441 using  $BVR_CI_C$  photometry and 44 epochs of phase-resolved optical spectroscopy. This paper is organized as follows. In Section 2, we describe the observations and data reduction. The analysis and results of the spectroscopic and photometric data are shown in Section 3. Section 4 discusses the masses and evolutionary status of the system. Finally, in Section 5, we summarize our results.

## 2 OBSERVATIONS AND DATA REDUCTION

### 2.1 Photometry

Photometric data for HS 2231+2441 in the  $B$ ,  $V$ ,  $R_C$  and  $I_C$  bands were collected between 2010 August and 2013 August using the facilities of Observatório do Pico dos Dias (OPD/LNA) in Brazil.

The observations were performed using an Ikon-L CCD camera attached to the 1.6-m and 0.6-m telescopes. To remove systematic effects from the CCD data, we collected typically  $\sim 30$  bias frames and  $\sim 30$  dome flat-field images on each night of observation. These observations are described in Table 1.

Data reduction was done using the usual IRAF tasks.<sup>1</sup> We built an automated computational procedure that subtracts a master median bias image from each program image and divides the result by a normalized flat-field frame. As the HS 2231+2441 field is not crowded, aperture differential photometry is a suitable technique for obtaining the relative magnitude between our target and a set of constant stars in the field. The result of this procedure can be seen in a sample of normalized light curves (see Fig. 1), folded on the orbital period of HS 2231+2441, which is derived in Section 3.1.2.

### 2.2 Spectroscopy

Raw spectroscopic data for HS 2231+2441 were retrieved from the Isaac Newton Group public archive.<sup>2</sup> The spectroscopic observations were performed with the ISIS spectrograph attached to the 4.2-m William Herschel Telescope at Roque de los Muchachos Observatory. 44 spectra were collected using the 600 l/mm grating and integration times of 5 and 10 min. The spectral coverage is 3600–5000 Å, with 0.45 Å full width at half-maximum (FWHM) resolution. Bias and flat-field images were collected each night to remove systematic signatures from the CCD detector. Wavelength calibration was done using a Cu-Ar comparison lamp for each night of observation. A summary of the observations is shown in Table 2.

The spectroscopic data reduction was done in the standard way using IRAF routines. The procedure includes bias subtraction, normalized flat-field division, optimal extraction and wavelength calibration. The average of all spectra after Doppler shifting according to the radial velocity orbital solution, see Section 3.2.1, is shown in Fig. 2.

## 3 ANALYSIS AND RESULTS

### 3.1 Differential photometry

#### 3.1.1 Light curves

The light curves of HS 2231+2441 (Fig. 1) are typical of HW Vir systems, i.e. they show a reflection effect and both primary and secondary eclipses. While the secondary eclipse depths increase towards longer wavelengths, from  $\sim 0.025$  mag in the  $B$  band to  $\sim 0.04$  mag in the  $I_C$  band, the primary ones do not change significantly with wavelength and are  $\sim 0.2$  mag in all bands.

#### 3.1.2 Ephemeris

The ephemeris for HS 2231+2441 was derived following the same procedure in Almeida, Jablonski & Rodrigues (2013). In short, we measure the mid-eclipse times by modelling the primary eclipse with the Wilson–Devinney code (WDC, version 2013) (Wilson, Van Hamme & Terrell 2010), which was implemented with a Markov

<sup>1</sup> IRAF is distributed by the National Optical Astronomy Observatories, which are operated by the Association of Universities for Research in Astronomy, Inc, under a cooperative agreement with the National Science Foundation.

<sup>2</sup> <http://casu.ast.cam.ac.uk/casuadc/ingarch/query>



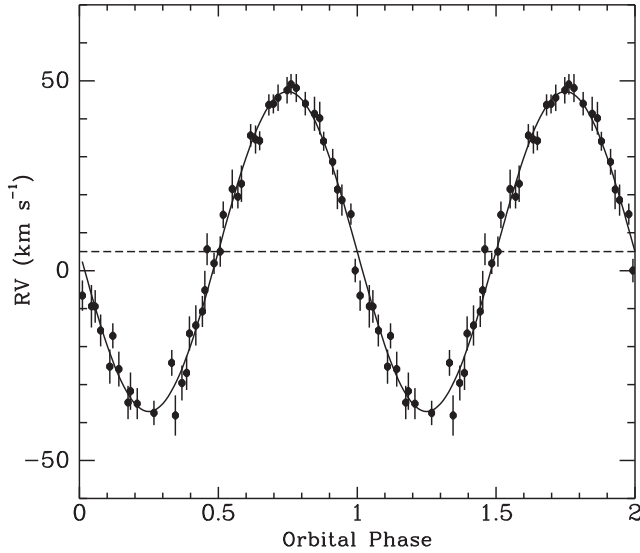


**Figure 3.** Radial velocities of the prominent lines in the spectra of HS 2231+2441 folded on the orbital period. The phases are calculated according to the ephemeris in equation (2). Solid and dashed lines represent the best radial velocity solution and systemic velocity, respectively.

52 values of effective temperatures in the range 25 000–35 000 K with 500 K steps, 16 surface gravities,  $5.2 \leq \log g \leq 6.0$ , with 0.05 dex steps, 10 He abundances,  $0.001 \leq n(\text{He})/n(\text{H}) \leq 0.01$ , with 0.0005 dex steps, and 20 projected rotational velocities,  $0 \leq v_{\text{rot}} \leq 200 \text{ km s}^{-1}$ , with  $10 \text{ km s}^{-1}$  steps.

To choose the synthetic spectrum that best matches the observed one, we convolved all synthetic spectra with the FWHM ( $0.5 \text{ \AA}$ ) of the instrumental profile obtained from the spectroscopic observation. The spectral regions around the Balmer ( $H\beta$  to  $H11$ ) and helium ( $\text{He I } \lambda 4026$  and  $\text{He I } \lambda 4471$ ) lines were used in the fitting procedure to determine the effective temperature, surface gravity, He abundance and rotational projected velocity. A minimization using the  $\chi^2$  technique was done in the last step. The best fit yields  $T_{\text{eff}} = 28\,500 \pm 500 \text{ K}$ ,  $\log g = 5.40 \pm 0.05$ ,  $\log(n(\text{He})/n(\text{H})) = -2.52 \pm 0.07$  and  $v_{\text{rot}} = 70 \pm 10 \text{ km s}^{-1}$ . The adopted error bar in each parameter is the step in its respective grid. With the exception of  $n(\text{He})/n(\text{H})$ , our results are in agreement with those obtained by Østensen et al. (2007, 2008). The projected velocity is consistent with a synchronized system, i.e.  $P_{\text{orb}} = P_{\text{rot}} = 2\pi R/v_{\text{rot}}$  (see Table 4). Fig. 4 shows the observed lines superimposed with the best synthetic spectrum.

### 3.3 Light and radial velocity curve analysis

Simultaneous modelling of multiband light curves and radial velocity curves is a powerful tool for deriving the geometrical and physical parameters of eclipsing binaries (see e.g. Wilson 1979; Almeida et al. 2012, 2015). We fitted the light curves in the  $B$ ,  $V$ ,  $R_C$  and  $I_C$  bands and the primary star radial velocity curve of the HS 2231+2441 binary using the latest version of wdc (Wilson et al. 2010). wdc is a generator of synthetic multiband light curves and radial velocity curves of binary systems. To optimise the fitting procedure, we incorporated the genetic algorithm PIKAIA (Charbonneau 1995) into wdc to search for a global solution and a MCMC procedure to sample around their expected values and obtain their uncertainties.

**Table 4.** System parameters of the best model fitted to photometric light curves in the  $B$ ,  $V$ ,  $R_C$  and  $I_C$  bands and the primary star radial velocity curve of HS 2231+2441.

Parameter	Value	
	Solution 1	Solution 2
<b>Fixed parameters</b>		
$q$ ( $M_2/M_1$ )	0.190	0.160
$T_1$ (K)	28 500	28 500
$\alpha_1^a$ ( $B$ )	0.290	0.290
$\alpha_1^a$ ( $V$ )	0.256	0.256
$\alpha_1^a$ ( $R_C$ )	0.222	0.222
$\alpha_1^a$ ( $I_C$ )	0.188	0.188
$\alpha_2^a$ ( $B$ )	0.727	0.677
$\alpha_2^a$ ( $V$ )	0.742	0.651
$\alpha_2^a$ ( $R_C$ )	0.705	0.624
$\alpha_2^a$ ( $I_C$ )	0.594	0.527
$\beta_1^b$	1	1
$\beta_2^b$	0.3	0.3
$A_1^c$	1	1
<b>Adjusted parameters</b>		
$\Omega_1^d$	$4.31 \pm 0.05$	$4.24 \pm 0.06$
$\Omega_2^d$	$2.91 \pm 0.03$	$2.68 \pm 0.02$
$T_2$ (K)	$3010 \pm 460$	$3410 \pm 500$
$i$ ( $^\circ$ )	$79.4 \pm 0.2$	$79.6 \pm 0.1$
$a^e$ ( $R_\odot$ )	$0.59 \pm 0.01$	$0.67 \pm 0.02$
$A_2^c$ ( $B$ )	$1.243 \pm 0.07$	$1.39 \pm 0.09$
$A_2^c$ ( $V$ )	$1.305 \pm 0.06$	$1.28 \pm 0.08$
$A_2^c$ ( $R_C$ )	$1.574 \pm 0.05$	$1.76 \pm 0.06$
$A_2^c$ ( $I_C$ )	$1.797 \pm 0.05$	$1.87 \pm 0.05$
<b>Derived parameters</b>		
$M_1$ ( $M_\odot$ )	$0.190 \pm 0.006$	$0.288 \pm 0.005$
$M_2$ ( $M_\odot$ )	$0.036 \pm 0.004$	$0.046 \pm 0.004$
$R_1$ ( $R_\odot$ )	$0.144 \pm 0.004$	$0.165 \pm 0.005$
$R_2$ ( $R_\odot$ )	$0.074 \pm 0.004$	$0.086 \pm 0.004$
$\log g_1$ ( $\text{cm s}^{-2}$ )	$5.40 \pm 0.03$	$5.46 \pm 0.03$
$\log g_2$ ( $\text{cm s}^{-2}$ )	$5.25 \pm 0.07$	$5.23 \pm 0.006$
$v_{\text{rot}, 1}^f$	$65.9 \pm 1.9$	$75.5 \pm 2.3$
$v_{\text{rot}, 2}^f$	$33.9 \pm 1.9$	$39.4 \pm 1.9$

<sup>a</sup>Linear limb darkening coefficient from Claret & Bloemen (2011); <sup>b</sup>gravity darkening exponent; <sup>c</sup>bolometric albedo; <sup>d</sup>adimensional potential; <sup>e</sup>component separation; <sup>f</sup>rotational velocity adopting synchronized rotation ( $P_{\text{orb}} = P_{\text{rot}}$ ).

The main parameters adjustable by wdc are the orbital period ( $P_{\text{orb}}$ ), epoch ( $T_0$ ), mass ratio ( $q = M_2/M_1$ ), inclination ( $i$ ), and the adimensional potentials and temperatures of both components ( $\Omega_1$ ,  $\Omega_2$ ,  $T_1$  and  $T_2$ ). However, wdc allows one to fit about 60 parameters, which refer to the physical and geometrical properties of the binary and also to a possible third component. Therefore, one needs to constrain them as much as possible with prior information from photometry, spectroscopy and theory. In our case, the orbital period and epoch are already known from the light curves (see Section 3.1.2). From the spectroscopic analysis, we derive the effective temperature of the primary star (see Section 3.2.2), and together with theoretical information, we can constrain  $q$  using  $K_1$  and the mass function,

$$f(m_2) = \frac{M_1(q \sin i)^3}{(1+q)^2} = \frac{(1-e^2)}{2\pi G} K_1^3 P_{\text{orb}}, \quad (3)$$

where  $G$  is the gravitational constant. We adopted the ranges  $0.1 M_\odot < M_1 < 0.8 M_\odot$  – which covers the mass range for sdBs, LMWDs and ELM white dwarfs (Heber 2016) – and  $75^\circ < i < 90^\circ$  to search for the primary mass and orbital inclination, respectively.

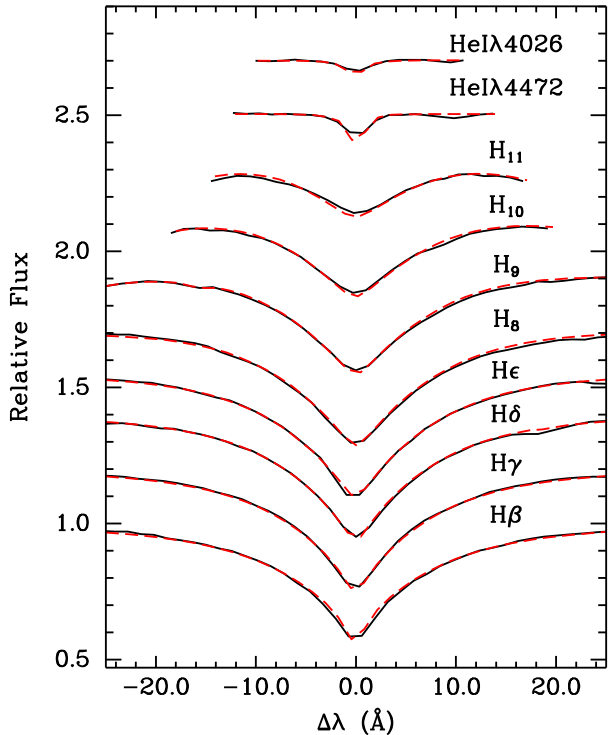


**Figure 4.** The best fit to the Balmer and helium lines used to derive the effective temperature, surface gravity, helium abundance and rotational velocity. The observed spectrum lines are presented with solid lines and the dashed lines represent the best synthetic spectra.

Assuming a circular orbit ( $e = 0$ ), the estimated mass ratio range is 0.11–0.25.

Although the orbital period is very short, the shape of its light curve shows a detached configuration. Therefore, wdc mode 2 is the most suitable because it does not constrain the Roche configuration. The luminosity of the secondary component was computed using stellar atmosphere radiation. The gravity darkening exponent ( $\beta_1$ ) and the bolometric albedo ( $A_1$ ) of the primary star were set to 1, while the gravity darkening exponent of the secondary component ( $\beta_2$ ) was fixed to 0.3 (Rafert & Twigg 1980). The linear limb darkening coefficients ( $\alpha$ ) from Claret & Bloemen (2011), which assume different values for the different photometric bands (see Table 4), were linearly extrapolated for both stars. As pointed out in previous studies (see e.g. For et al. 2010; Almeida et al. 2012), the albedo of the secondary star in HW Vir systems can assume non-physical values, i.e.  $A_2 > 1$ . This happens because the reflected-reradiated spectral energy rate from the secondary star increases towards longer wavelengths and may reach values greater than 1. To take this effect into account, we adopted the secondary albedo in all bands as a free parameter.

Finally, the remaining adjustable parameters for HS 2231+2441 are the mass ratio, orbital inclination, separation between the components ( $a$ ), the adimensional potentials and effective temperature of the secondary. However, as the mass ratio is highly correlated with the other parameters (see e.g. Schaffenroth et al. 2014, 2015), we performed a grid of solutions keeping  $q$  fixed. The grid has steps of 0.01 in mass ratio covering the range mentioned above. The models for different  $q$  have very similar chi-square values and the choice of the most probable solutions was done as described below. Fig. 5 compares the surface gravity of the wdc fitting (the photomet-

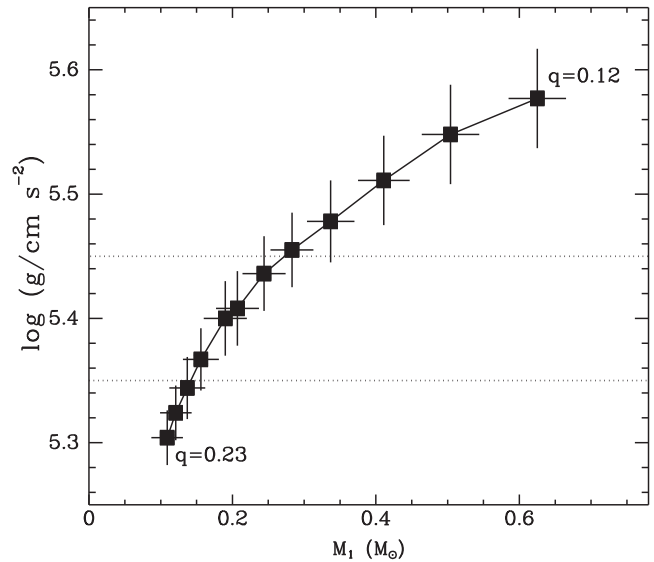


**Figure 5.** wdc solutions for surface gravity and mass of the primary star using fixed values of  $q$  are represented by squares. Horizontal dotted lines represent the lower and upper limits to the surface gravity derived from the spectroscopic modelling. The photometric and spectroscopic surface gravities are equal for  $q = 0.19$ .

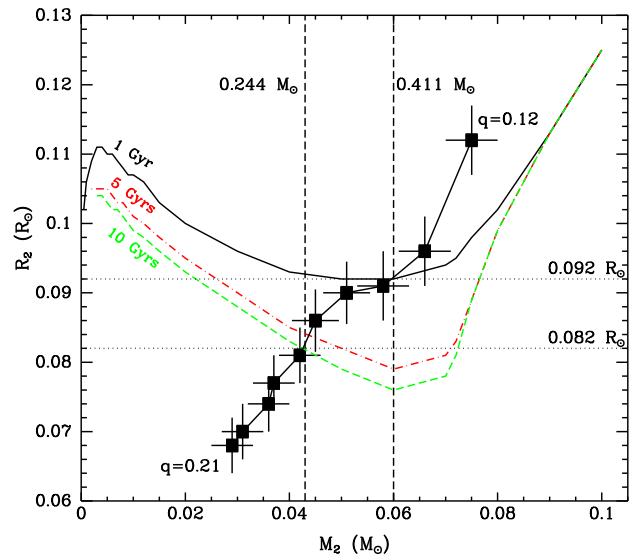


**Figure 6.** Mass versus radius relationship for low-mass and brown dwarf stars. wdc solutions for the secondary mass and radius using fixed values of  $q$  are shown using squares. Theoretical mass versus radius relationships for 1, 5 and 10 Gyr calculated by Baraffe et al. (2003) are shown with solid, dash-dotted and dashed lines, respectively. Horizontal dotted and vertical dashed lines represent the lower and upper limits for the secondary radius and the primary mass considering the possible theoretical range for the mass and radius of the secondary star, respectively.

ric solution) with that obtained from the spectral line profiles (the spectroscopic solution). The photometric solution coincides with the spectroscopic one for  $q = 0.19$ . A different approach is presented in Fig. 6, which shows the secondary mass and radius from the photometric solutions and the theoretical models for low-mass stars and brown dwarfs from Baraffe et al. (2003). The solutions are consistent with the models for  $0.14 < q < 0.17$ . Considering that the age for compact hot stars with a progenitor less massive than

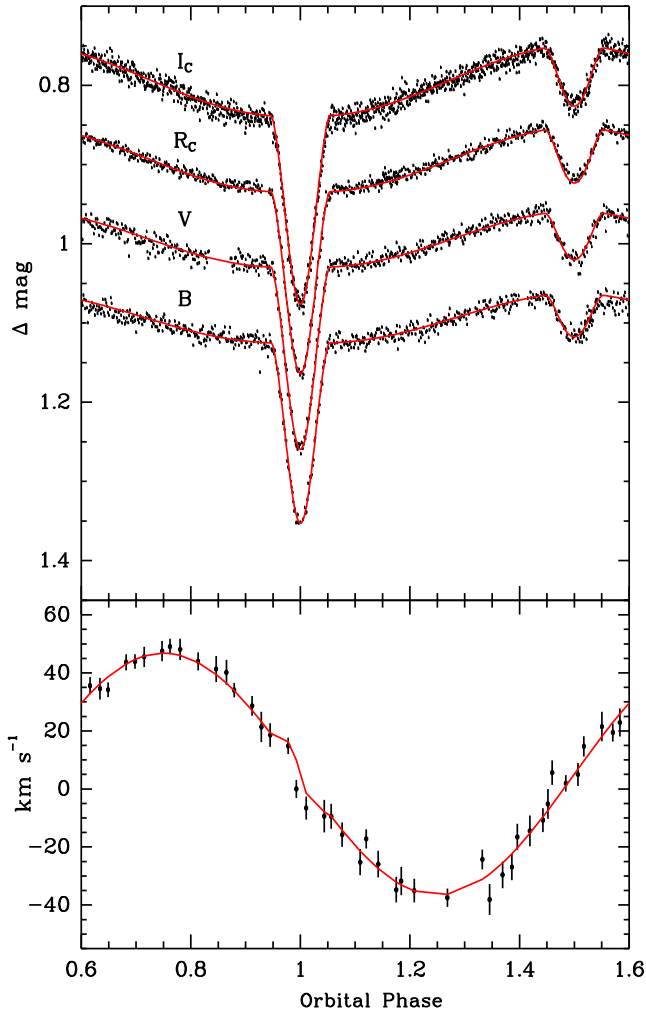


**Figure 7.** The best simultaneous fits to the light curves in the  $B$ ,  $V$ ,  $R_C$  and  $I_C$  bands and primary radial velocity curve performed with `wc`.

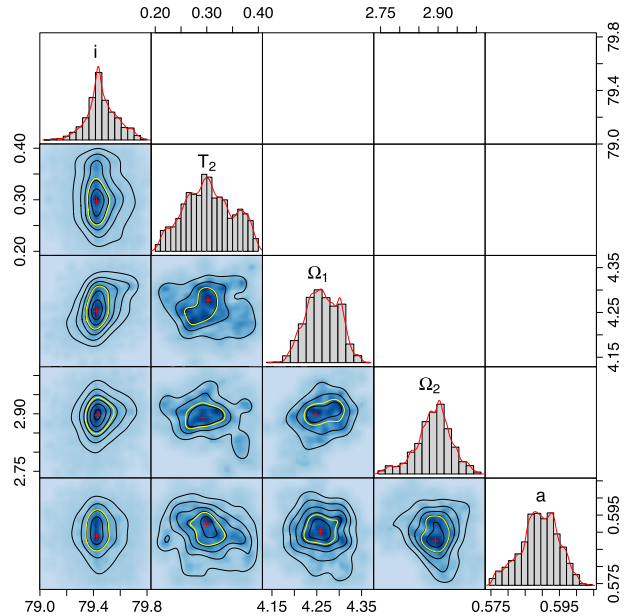
$1.2 M_{\odot}$  is larger than 5 Gyr (Schindler, Green & Arnett 2015), the most plausible solution is obtained with  $q = 0.16$ . Therefore, we list the fitted and derived parameters for these two solutions in Table 4.

Fig. 7 shows the best fit for  $q = 0.19$  together with the light curves for the  $B$ ,  $V$ ,  $R_C$ , and  $I_C$  bands and the primary radial velocity curve. Both solutions have indistinguishable fits and  $\chi_{\text{red}}^2 = 1.03$ . Fig. 7 (bottom panel) shows a feature visible between the phases 0.95 and 1.05, like a sinusoidal curve superimposed on the radial velocity curve. This is known as the Rossiter–McLaughlin effect and occurs when the secondary passes in front of a rotating primary and vice versa, if both stars are visible (Ohta, Taruya & Suto 2005). In our fitting, we take this effect into account, adopting the simplified case, i.e. a circular orbit and synchronized and corotational components. As an example, Fig. 8 shows the a posteriori probability densities of the main fitted parameters for the solution obtained with  $q = 0.19$ .

## 4 DISCUSSION

### 4.1 Evolution status of the primary star

According to Han et al. (2003), the primary star in *HW Vir* systems can be formed in the following channel. The two components of the binary are on the main sequence and the primary is the most



**Figure 8.** Joint distributions of the a posteriori probability densities for the main parameters fitted in the simultaneous analysis of the HS 2231+2441 light and radial curves. Our MCMC has  $2 \times 10^4$  iterations sampling the regions around the best solution obtained with  $q = 0.19$  found by the `PIKAIA` algorithm.

massive. When the primary ascends to the red giant branch (RGB), a dynamic mass transfer begins. This leads to the common envelope and a spiral-in phase. The primary envelope absorbs the released gravitational potential energy and it is subsequently ejected. The sdB star develops if the core of the giant still burns helium. The final result is a short-period binary with a sdB plus a main sequence companion.

In the channel discussed above, the resultant sdB star will have a mass larger than  $\sim 0.47 M_{\odot}$ , which is the lower limit needed to ignite the helium in its core (Han et al. 2003). However, a LMWD or an ELM white dwarf star can be formed through the so-called post-RGB scenario (Driebe et al. 1998; Han et al. 2003). This channel occurs when the remaining mass of the primary after the first common-envelope phase is insufficient to ignite helium.

To check which evolutionary model is the most likely for the HS 2231+2441 primary star, we use the  $\log g$  versus effective temperature ( $T_{\text{eff}}$ ) diagram. Fig. 9 shows the location of the primary component of HS 2231+2441, some primary stars in *HW Vir* systems, and a sample of single sdB stars, as presented in Edelmann (2003). Post-EHB and post-RGB evolutionary tracks from Dorman (1993) and Driebe et al. (1998), respectively, are also shown. Considering the mass derived for the primary star in both solutions (see Table 4), the most plausible scenario is the post-RGB evolutionary track placing the HS 2231+2441 primary star in the LMWD or ELM white-dwarf regime.

### 4.2 Masses of the HS 2231+2441 components

In recent years, several dozen of these LMWDs and ELM white dwarfs have been reported in the literature (see e.g. Rebassa-Mansergas et al. 2011; Gianninas et al. 2014a,b). These objects were found as part of binary systems and their companions can be of several types, e.g. neutron stars, white dwarfs and main sequence stars (see e.g. Gianninas et al. 2014a; Brown et al. 2016;

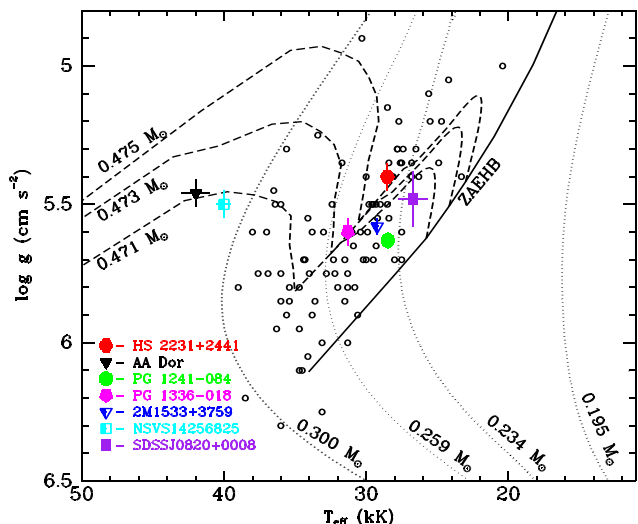


**Figure 9.** Location of the HS 2231+2441 primary star in the  $T_{\text{eff}}$  versus  $\log g$  diagram. A few primary stars in HW Vir systems are shown with different symbols (see legend). Open circles represent isolated sdB stars from Edelmann (2003). Evolutionary tracks to different masses in the post-EHB evolution (Dorman 1993) and post-RGB evolution (Driebe et al. 1998) are shown with dashed and dotted lines, respectively. The solid line represents zero age at the EHB.

Heber 2016). The first reported ELM white dwarf is the companion of a neutron star in the millisecond pulsar PSR J1012+5307 (van Kerkwijk, Bergeron & Kulkarni 1996). Later, Driebe et al. (1998) determined the mass of this object as  $M = 0.19 \pm 0.02 M_{\odot}$ . Rebassa-Mansergas et al. (2011) compared the mass distribution of post-common-envelope binaries and wide white dwarf plus main sequence binaries from the Sloan Digital Sky Survey and confirmed that the majority of LMWDs reside in close binary systems. They showed that, even though the mass distribution of the whole sample displays two peaks near  $0.55 M_{\odot}$  and  $0.4 M_{\odot}$ , the mass distribution of the post-common-envelope binaries has a concentration of systems towards the low-mass side. Heber (2016) suggested that the ELM white dwarfs and LMWDs have masses around  $0.2$  and  $0.3 M_{\odot}$ , respectively. Therefore, both solutions for HS 2231+2441, which provide a primary mass of  $0.19 M_{\odot}$  and  $0.288 M_{\odot}$  (see Table 4), place the primary component as either an ELM white dwarf or a LMWD.

The confirmed dM-star/brown dwarf companions in HW Vir systems have a mass distribution concentrated around  $0.1 M_{\odot}$  (Kupfer et al. 2015). In the lower part of the mass distribution, there are a few cases with confirmed brown dwarfs: SDSS J162256+473051, SDSS J082053.53+000843.4 and V2008-1753, which have secondary masses of  $0.060 M_{\odot}$  (Schaffenroth et al. 2014),  $0.068 M_{\odot}$  (Geier et al. 2011) and  $0.047 M_{\odot}$  (Schaffenroth et al. 2015), respectively. Thus, the secondary star of HS 2231+2441, considering both solutions, has one of the lowest masses,  $\sim 0.036$  and  $\sim 0.046 M_{\odot}$ , for a companion object in the HW Vir systems known so far.

If we assume the sdB canonical mass ( $0.47 M_{\odot}$ ) for the HS 2231+2441 primary, the mass ratio would be approximately equal to  $0.135$ . The surface gravity of the primary would be  $\log g \sim 5.53$ , which is in disagreement with the measured spectroscopic surface gravity (Fig. 5). Moreover, the radius of the secondary star would be much larger ( $\sim 0.094 R_{\odot}$ ) than that expected from the theoretical mass versus radius relationship (see Fig. 6).

The mass of the secondary component would be  $0.063 M_{\odot}$ , still consistent with a brown dwarf.

## 5 SUMMARY

In this study, we characterize the HW Vir system HS 2231+2441 using photometric and spectroscopic data. This system has a short orbital period,  $P_{\text{orb}} = 0.11$  d, and shows a typical HW Vir light curve, i.e. both primary and secondary eclipses and the reflection effect. A spectroscopic analysis enabled us to derive the following properties of the HS 2231+2441 primary: the semi-amplitude of the radial velocity curve,  $42 \pm 1.0 \text{ km s}^{-1}$ , the effective temperature,  $T_{\text{eff}} = 28500 \pm 500 \text{ K}$ , the surface gravity,  $\log g = 5.40 \pm 0.05$ , and the helium abundance,  $\log(n(\text{He})/n(\text{H})) = -2.52 \pm 0.07$ . Furthermore, we derive the projected rotational velocity,  $v_{\text{rot}} = 70 \pm 10 \text{ km s}^{-1}$ , which is consistent with a synchronized system.

Using nine eclipse timings spread over 1100 d, we derived a new linear ephemeris for HS 2231+2441. The residuals with respect to this fit do not show any evidence of an orbital period variation.

We derived the main parameters of HS 2231+2441 (see Table 4) by modelling the  $B$ ,  $V$ ,  $R_C$  and  $I_C$  band light curves and the primary radial velocity curve using wdc. Solutions with a mass ratio equal to  $0.19$  and  $0.16$  were found to be the most probable considering the measured photometric and spectroscopic surface gravity of the primary star and the derived mass and radius of the secondary star in comparison with the theoretical mass versus radius relationship for low-mass and brown dwarf stars. Both solutions yield a primary component with low mass ( $0.19 M_{\odot}$  or  $0.288 M_{\odot}$ ) and a secondary star in the brown dwarf regime ( $0.036 M_{\odot}$  or  $0.046 M_{\odot}$ ). These masses agree with the results obtained by Østensen et al. (2008).

The evolutionary status of the primary star in HS 2231+2441 was analysed using the effective temperature versus surface gravity diagram. Comparing the location of the primary in this diagram with post-RGB and post-EHB evolutionary tracks, we concluded that the post-RGB scenario is most likely for the HS 2231+2441 primary star.

Thus, HS 2231+2441 has either an ELM white dwarf or a LMWD plus a brown dwarf star. The secondary star has one of the lowest masses found among the HW Vir systems (see e.g. Almeida et al. 2012; Kupfer et al. 2015). This system may represent the close binaries composed of a LMWD ( $< 0.5 M_{\odot}$ ) plus a main sequence low-mass object discovered in large numbers by Rebassa-Mansergas et al. (2011).

## ACKNOWLEDGEMENTS

The authors thank the anonymous referee for helpful suggestions. This study was partially supported by Fundação de Amparo à Pesquisa do Estado de São Paulo (LAA: 2012/09716-6 and 2013/18245-0; AD: 2011/51680-6 and CVR: 2013/26258-4), Conselho Nacional de Desenvolvimento Científico e Tecnológico (CVR: 306701/2015-4) and Coordenação de Aperfeiçoamento de Pessoal de Nível Superior. This paper makes use of data obtained from the Isaac Newton Group Archive, which is maintained as part of the Cambridge Astronomy Survey Unit Astronomical Data Centre at the Institute of Astronomy, Cambridge. The TheoSSA service (<http://dc.g-vo.org/theossa>) used to retrieve theoretical spectra for this paper was constructed as part of the activities of the German Astrophysical Virtual Observatory.

## REFERENCES

- Almeida L. A., Jablonski F., Tello J., Rodrigues C. V., 2012, *MNRAS*, 423, 478
- Almeida L. A., Jablonski F., Rodrigues C. V., 2013, *ApJ*, 766, 11
- Almeida L. A. et al., 2015, *ApJ*, 812, 102
- Baraffe I., Chabrier G., Barman T. S., Allard F., Hauschildt P. H., 2003, *A&A*, 402, 701
- Brown W. R., Kilic M., Allende Prieto C., Kenyon S. J., 2010, *ApJ*, 723, 1072
- Brown W. R., Gianninas A., Kilic M., Kenyon S. J., Allende Prieto C., 2016, *ApJ*, 818, 155
- Charbonneau P., 1995, *ApJS*, 101, 309
- Claret A., Bloemen S., 2011, *A&A*, 529, A75
- Dorman B., 1993, *ApJ*, 419, 596
- Driebe T., Schoenberner D., Bloeker T., Herwig F., 1998, *A&A*, 339, 123
- Edelmann H., 2003, *A&A*, 400, 939E
- For B.-Q. et al., 2010, *ApJ*, 708, 253
- Geier S. et al., 2011, *ApJ*, 731, L22
- Gianninas A., Hermes J. J., Brown W. R., Dufour P., Barber S. D., Kilic M., Kenyon S. J., Harrold S. T., 2014a, *ApJ*, 781, 104
- Gianninas A., Dufour P., Kilic M., Brown W. R., Bergeron P., Hermes J. J., 2014b, *ApJ*, 794, 35
- Han Z., Podsiadlowski P., Maxted P. F. L., Marsh T. R., Ivanova N., 2002, *MNRAS*, 336, 449
- Han Z., Podsiadlowski Ph., Maxted P. F. L., Marsh T. R., 2003, *MNRAS*, 341, 669
- Heber U., 2016, *PASP*, 128, 082001
- Kupfer T. et al., 2015, *A&A*, 576, A44
- Ohta Y., Taruya A., Suto Y., 2005, *ApJ*, 622, 1118
- Østensen R., Oreiro R., Drechsel H., Heber U., Baran A., Pigulski A., 2007, *ASP Conf. Ser.*, 372, 483
- Østensen R. H., Oreiro R., Hu H., Drechsel H., Heber U., 2008, *ASP Conf. Ser.*, 392, 221
- Østensen R. H. et al., 2013, *A&A*, 559, A35
- Rafert J. B., Twigg L. W., 1980, *MNRAS*, 193, 79
- Rebassa-Mansergas A., Nebot Gómez-Morán A., Schreiber M. R., Girven J., Gänsicke B. T., 2011, *MNRAS*, 413, 1121
- Schafferoth V., Geier S., Heber U., Kupfer T., Ziegerer E., Heuser C., Classen L., Cordes O., 2014, *A&A*, 564, A98
- Schafferoth V., Barlow B. N., Drechsel H., Dunlap B. H., 2015, *A&A*, 576, A123
- Schindler J.-T., Green E. M., Arnett W. D., 2015, *ApJ*, 806, 178
- Taam R. E., Sandquist E. L., 2000, *ARA&A*, 38, 113
- van Kerkwijk M. H., Bergeron P., Kulkarni S. R., 1996, *ApJ*, 467, L89
- Wilson R. E., 1979, *ApJ*, 234, 1054
- Wilson R. E., Van Hamme W., Terrell D., 2010, *ApJ*, 723, 1469

This paper has been typeset from a  $\text{\TeX}/\text{\LaTeX}$  file prepared by the author.